

ICCE Report B/197/2015

February 2015

**Multigrid method and mixed FEM in multiscale  
modeling of coupled problems**

**Witold Cecot, Marta Oleksy**

This research was supported by the National Science Center under grant  
2011/01/B/ST6/07312.

Institute for Computational Civil Engineering  
Faculty of Civil Engineering  
Cracow University of Technology



# Contents

<b>1</b>	<b>Summary</b>	<b>3</b>
<b>2</b>	<b>Multigrid based homogenization</b>	<b>5</b>
2.1	Introduction . . . . .	5
2.2	Multigrid homogenization with a new interpolation operator . .	6
2.3	Numerical examples . . . . .	8
2.4	Coupled problems . . . . .	14
2.5	Numerical examples . . . . .	15
<b>3</b>	<b>Mixed finite elements</b>	<b>19</b>
3.1	Two-dimensional mixed hp-finite elements . . . . .	19
3.2	Edge functions . . . . .	21
3.3	Bubble functions . . . . .	22
3.4	Numerical tests . . . . .	23
<b>4</b>	<b>Concluding remarks</b>	<b>26</b>
	<b>Bibliography</b>	<b>27</b>

# Chapter 1

## Summary

Two issues related to numerical homogenization are addressed in this report. Firstly, we present application of the multigrid homogenization to coupled thermo-mechanical problems. Secondly the preliminary study of advantages of mixed formulation based elastic-plastic analysis is discussed.

In the last years the most intensively used method for analysis of multi-scale problems is the computational homogenization (also called the global - local analysis) [18] that enables determination of global material parameters of heterogeneous body on the basis of reduced, in an appropriate way, data from the micro-scale.

In our research, presented in this report, we develop the multigrid homogenization [16], which may be used for both periodic and non-periodic materials. Typically, first order shape functions are used. Only recently higher order Lagrange type bases were successfully applied and presented in paper [24]. However, convergence of the results only for the Laplace operator in L2 norm for approximation of up to the second order was studied therein. The bubble function based, higher order FEM approximation and a new, improved definition of the inter grid operator for the linear elasticity, which lead to a fast convergence of both displacements and stresses, were proposed by us in [11]. Contrary to the previous approaches the right-hand sides of the local boundary value problems that define mappings, were assumed as the regular parts of certain residues rather than arbitrarily assumed polynomials. Recently we also extended and tested that improvement for the thermo-mechanical problems. Our main contributions consist of the improved, appropriate for bubble functions of arbitrary order, inter grid mapping as well as an experimental confirmation of a fast, even exponential, convergence of both displacements

and stresses for the linear elasticity and the coupled thermo-mechanical problems. Particularly, the high accuracy of homogenized solution derivatives and efficiency of their computation are the important advantages of the improved multigrid homogenization in comparison with other multiscale techniques.

The mixed FEM was also discussed due to the same convergence rate for displacements and stresses. The  $H_{\text{div}}$  class shape functions were constructed in two ways leading to fast convergence for solid mechanics with or without plastic strains. Thus, it is of particular interest for heterogeneous materials or elastic-plastic analysis.

## Chapter 2

# Multigrid based homogenization

### 2.1 Introduction

In the last years the most intensively used method for analysis of multiscale problems is the computational homogenization. In our research we develop the multigrid homogenization, which may be used for both periodic and non-periodic materials. The higher order FEM approximation at the macro-scale and a new definition of the intergrid operators leading to a fast convergence of both displacements and stresses was proposed in [11]. In fact only two meshes were used, fine one that resolves locally the highly oscillating material properties and a coarse mesh for global, low cost computation. Thus, it results in evaluation of the mean global field as well as local fluctuations of both displacements and stresses.

Generally, the multigrid method [8] may be used in two different ways for heterogeneous materials. Either, in a special version accommodated for fast varying material parameters in order to obtain efficiently a direct numerical solution on the most fine grid [1, 20] or as an upscaling method [16, 19, 21, 7] leading to homogenized solution on the coarsest mesh. The later method is equivalent to the Multiscale FEM (MsFEM) [14, 24], in which special shape functions are constructed to resolve all the details of material heterogeneities. Typically first order shape functions are used. Only recently Soghrati and Stanciulescu [24] used higher order Lagrange type bases, however they studied convergence only in  $L_2$  norm for approximation of up to the second order.

## 2.2 Multigrid homogenization with a new interpolation operator

We present in this section the basic idea of the multigrid homogenization after [11]. Let's consider the well known linear elasticity problem with heterogeneous material: *find field of displacements  $\mathbf{u}(\mathbf{x})$  such that:*

$$-\frac{\partial}{\partial x_j} \left( C_{ijkl}^\varepsilon \frac{\partial u_k}{\partial x_l} \right) = f_i \quad \forall \omega_s \subset \Omega \quad (2.1)$$

with Dirichlet ( $\hat{\mathbf{u}}$ ) and Neumann ( $\hat{\mathbf{t}}$ ) boundary conditions on  $\partial\Omega_D$  and  $\partial\Omega_N$  respectively ( $\partial\Omega_D \cup \partial\Omega_N = \partial\Omega$ ,  $\partial\Omega_D \cap \partial\Omega_N = \emptyset$ ) as well as continuity conditions at the possible material interfaces  $\Gamma$ . We shall also assume  $L^2$  regularity of  $\mathbf{f}$ , strong ellipticity and boundedness of the material parameter tensor  $C^\varepsilon$ .

The weak displacement formulation of problem (2.1) is as follows: *find field of displacements  $\mathbf{u}(\mathbf{x}) \in V_0 + \hat{\mathbf{u}}$ , such that:*

$$\int_{\Omega} \boldsymbol{\sigma}(\mathbf{u}) : \boldsymbol{\varepsilon}(\mathbf{v}) \, d\Omega = \int_{\Omega} \mathbf{f} \cdot \mathbf{v} \, d\Omega + \int_{\partial\Omega_N} \hat{\mathbf{t}} \cdot \mathbf{v} \, ds \quad \forall \mathbf{v} \in V_0 \quad (2.2)$$

where  $V_0 = \{\mathbf{v} \in [H^1(\Omega)]^n, \mathbf{v} = 0 \text{ on } \partial\Omega_D\}$ .

Let the FEM system of algebraic equations be written in the following matrix form

$$\mathbf{K}^h \mathbf{u}^h = \mathbf{f}^h \quad (2.3)$$

where  $\mathbf{u}^h$  is the vector of dof and  $\mathbf{K}^h, \mathbf{f}^h$  denote the assembled matrix and vector.

Since solution of (2.3) may be computationally too expensive one may want to approximate it by a coarse mesh solution ( $\mathbf{u}^H$ ) defined by the following linear equations

$$\mathbf{K}^H \mathbf{u}^H = \mathbf{f}^H \quad (2.4)$$

However, the system (2.3) and consequently the dof vector ( $\mathbf{u}^H$ ) must account, at least implicitly, for the material heterogeneity, e.g. by the multigrid based homogenization. It is an "inverted" version of multigrid method since its primary objective is the coarse rather than fine mesh solution.

Similarly as in the multigrid method, the key components of the multigrid homogenization are  $\mathbf{I}$  and  $\mathbf{R}$  mappings between fine and coarse meshes. We proposed [11] to compute the  $\mathbf{I}$  operator as the solution of the following

boundary value problem defined for every coarse mesh element  $L_H$ : given  $\boldsymbol{\psi}$ , find  $\boldsymbol{\varphi}$  such that

$$\begin{aligned} \frac{\partial}{\partial x_i} C_{ijkl} \frac{\partial \Phi_k}{\partial x_l} &= \text{Reg} \left( \frac{\partial}{\partial x_i} C_{ijkl} \frac{\partial \Psi_k}{\partial x_l} \right) \quad \forall i = 1, 2, \mathbf{x} \in L \\ \Phi &= \hat{\Phi} \text{ on } \partial L \end{aligned} \quad (2.5)$$

where  $\hat{\Phi}$  consists of scalar valued functions obtained for every nonzero trace of all coarse element scalar shape functions  $\psi$  as the solution to the following 1D boundary value problem

$$\begin{aligned} \frac{d}{ds} (2\mu + \lambda) \frac{d\hat{\varphi}}{ds} &= \text{Reg} \left[ \frac{d}{ds} (2\mu + \lambda) \frac{\psi}{ds} \right] \quad \forall s \in (0, l) \\ \hat{\varphi}(0) &= \psi(0), \quad \hat{\varphi}(l) = \psi(l) \end{aligned} \quad (2.6)$$

where  $\text{Reg}$  denotes regular part of the derivative, i.e. without distributional part and  $s \in [0, l]$  stands for the parameter that defines an edge. The coefficient  $2\mu + \lambda$  represents material properties along an edge. It is worth mentioning that in some papers [17] instead of the edge problem (2.16) an oversampled domain (containing  $L_H$ ) in problem (??) is used to avoid the boundary layer effect.

In practice  $\Phi$  interpolants are computed numerically using the fine mesh that complies with the material distribution and equation (2.5) may be interpreted as equality of residuals in interiors of all finite elements. The corresponding weak form reads  $\boldsymbol{\Phi}(\mathbf{x}) \in V_0 + \boldsymbol{\Psi}$ ,

$$\int_{\Omega} \boldsymbol{\sigma}(\boldsymbol{\Phi}) : \boldsymbol{\varepsilon}(\mathbf{v}) \, d\Omega = \int_{\Omega} \mathbf{v} \cdot \text{Reg}[\text{div} \boldsymbol{\sigma}(\boldsymbol{\Psi})] \, d\Omega \quad \forall \mathbf{v} \in V_0 \quad (2.7)$$

and defines interpolation operator that transfers  $M$  coarse element degrees of freedom (dof) into  $N$  fine mesh dof. Such a mapping is represented by a matrix  $\mathbf{I}_{N \times M}$  and is used to compute the coarse element matrix  $\mathbf{K}^H$ , vector  $\mathbf{F}^H$  and the fine mesh dof  $\mathbf{u}^h$ , whenever the coarse mesh dof vector  $\mathbf{u}^H$  is known, namely

$$\mathbf{K}^H = \mathbf{I}^T \mathbf{K}^h \mathbf{I}, \quad \mathbf{F}^H = \mathbf{I}^T \mathbf{F}^h, \quad \mathbf{u}^h = \mathbf{I} \mathbf{u}^H \quad (2.8)$$

where  $\mathbf{K}^h$  denotes fine mesh, assembled only in coarse element domain  $L_H$ , stiffness matrix. The relations (2.8)<sub>1</sub>, (2.8)<sub>2</sub> may be easily proved defining errors of the solutions of the systems of algebraic equations for two meshes

$$\mathbf{e}^h = \mathbf{u} - \mathbf{u}^h, \quad \mathbf{e}^H = \mathbf{u} - \mathbf{u}^H \quad (2.9)$$

and the corresponding residual vectors

$$\mathbf{r}^h = \mathbf{f}^h - \mathbf{K}^h \mathbf{u}^h, \quad \mathbf{r}^H = \mathbf{f}^H - \mathbf{K}^H \mathbf{u}^H, \quad \mathbf{r}^H = \mathbf{R} \mathbf{r}^h \quad (2.10)$$

Thus,

$$\mathbf{K}^h \mathbf{u}^h = \mathbf{r}^h, \quad \mathbf{K}^H \mathbf{u}^H = \mathbf{r}^H \quad (2.11)$$

and since

$$\mathbf{r}^H = \mathbf{R} \mathbf{r}^h = \mathbf{R} \mathbf{K}^h \mathbf{e}^h = \mathbf{R} \mathbf{K}^h \mathbf{I} \mathbf{e}^H \quad (2.12)$$

as well as

$$\mathbf{f}^H = \mathbf{r}^H + \mathbf{K}^H \mathbf{u}^H = \mathbf{R} \mathbf{r}^h + \mathbf{R} \mathbf{K}^h \mathbf{I} \mathbf{u}^H = \mathbf{R} \mathbf{f}^h \quad (2.13)$$

and assuming, for the sake of  $\mathbf{K}^H$  symmetry, that  $\mathbf{R} = \mathbf{I}^T$  one obtains properties (2.8)<sub>1</sub>, (2.8)<sub>2</sub>. It is worth mentioning that they enable computation of coarse element meshes and vectors without additional numerical integration.

Construction of operator based interpolation is on the other hand exactly the same procedure as construction of special shape functions in the methods proposed by Babuška et al.[6] and developed by Hou and Wu in late nineties [17] as so called the multiscale FEM (MsFEM). The method was further developed by Efendiev and Hou [15] as well as Soghrati and Stanculescu [24].

## 2.3 Numerical examples

In this section we present results of experimentally studied accuracy and convergence for high order FEM in multigrid homogenization.

As a first 2D example we considered a square plate with a circular hole (Fig. 2.1). It was analyzed both directly to compute  $\mathbf{u}^h$  and by the presented approach to obtain the homogenized  $\mathbf{u}^H$  substitute. Only one coarse element, with shape functions of order varying from 1 to 5, was used and the fine mesh consisted of linear triangular elements. Comparison of the stresses obtained by both approaches (i.e. direct one and multigrid homogenization for  $p = 3$ ) is shown in Fig. 2.2 confirming qualitatively very good accuracy of the method. The convergence of modeling error for p-enrichment of the macro element is presented in Fig. 2.3.

In the second test the quality of homogenized solution was studied for various discretization at micro and macro levels for both displacements and stresses. A square domain with a circular inclusion shown in Fig. 2.4 was assumed as the test problem.

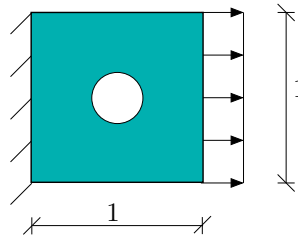


Figure 2.1: A unit square. Domain and boundary conditions

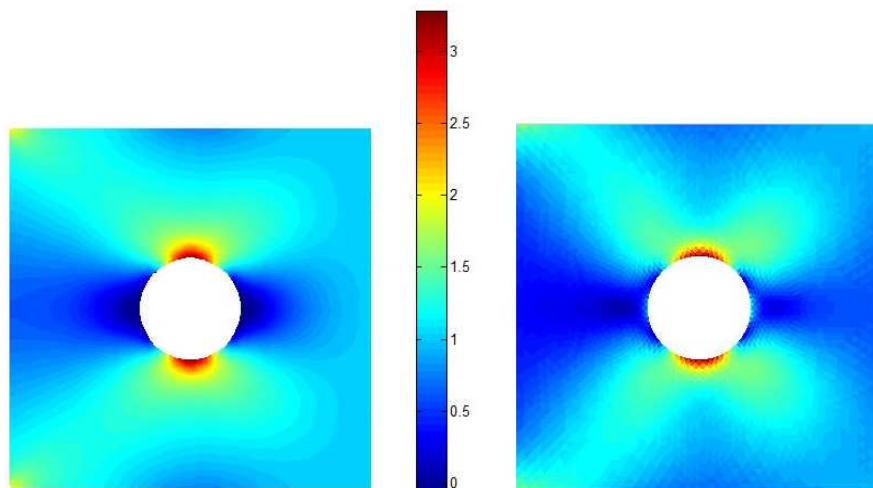


Figure 2.2: A unit square. Colour maps of exact (1400 dof) and homogenized stress  $\sigma_{xx}$  obtained by 50 dof

Displacements and stresses computed either by the direct approach, i.e. using the fine mesh, or by multigrid homogenization are compared in Figs 2.5-2.8. One finite element of the third order of approximation with 32 dof was used at the macroscale. It enabled to reconstruct with satisfactory quality displacements and stresses of the fine meshes that consisted of triangular linear elements with 60 to 2900 dof.

In the last test presented in this section the circle-like inclusions were centered at vertices of the square domain. Comparison of displacements and

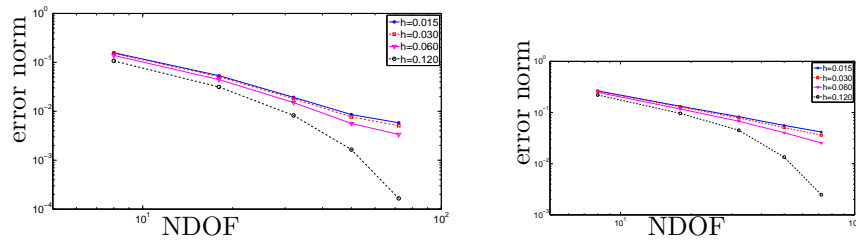


Figure 2.3: A unit square. Convergence in  $L_2$  and energy norms

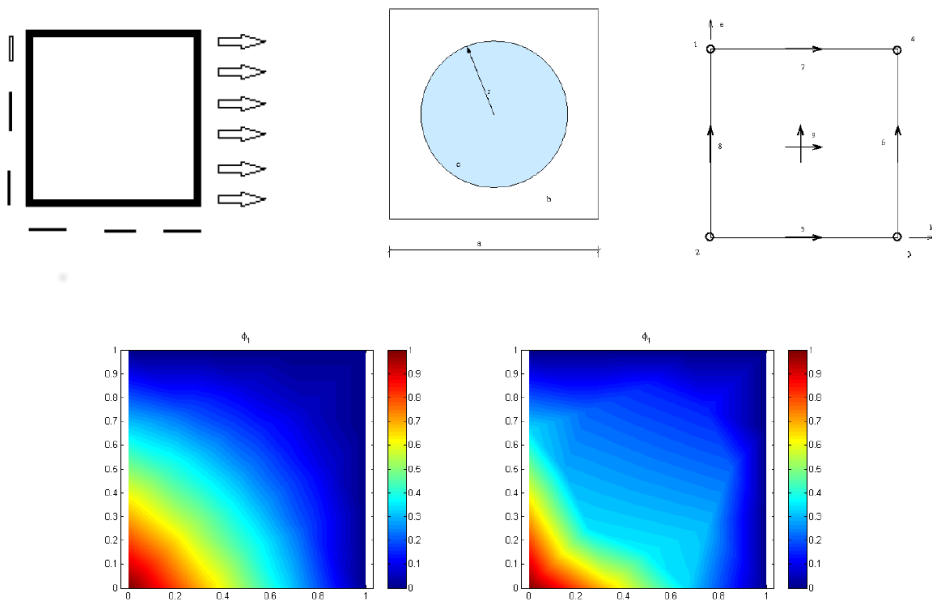


Figure 2.4: Test 2. First row - the domain with boundary conditions, material distribution and macro scale discretization by one quadrilateral element of 1st-3rd order of approximation. Second row - fine mesh interpolant of the first shape function for homogeneous and heterogeneous materials.

stresses, shown in Fig. 2.9, once more shows that the multigrid based homogenization with the new interpolation operator delivers reasonable results.

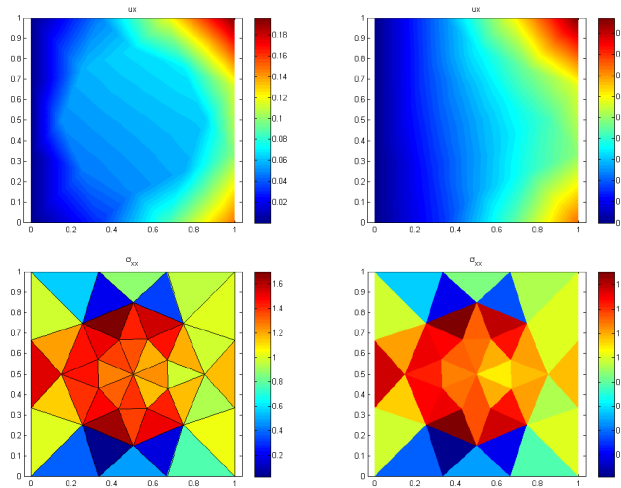


Figure 2.5: Test 2. Displacements (top row) and stresses (bottom row) obtained by fine mesh with 60 (left column) and coarse mesh with 32 (right column) dof.

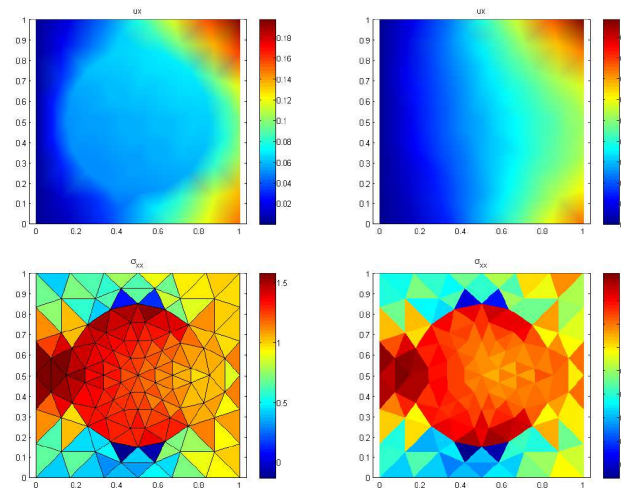


Figure 2.6: Test 2. Displacements (top row) and stresses (bottom row) obtained by fine mesh with 200 (left column) and coarse mesh with 32 (right column) dof.

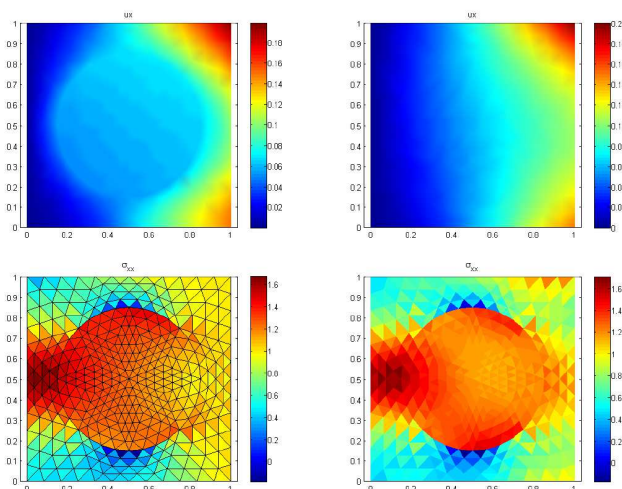


Figure 2.7: Test 2. Displacements (top row) and stresses (bottom row) obtained by fine mesh with 750 (left column) and coarse mesh with 32 (right column) dof.

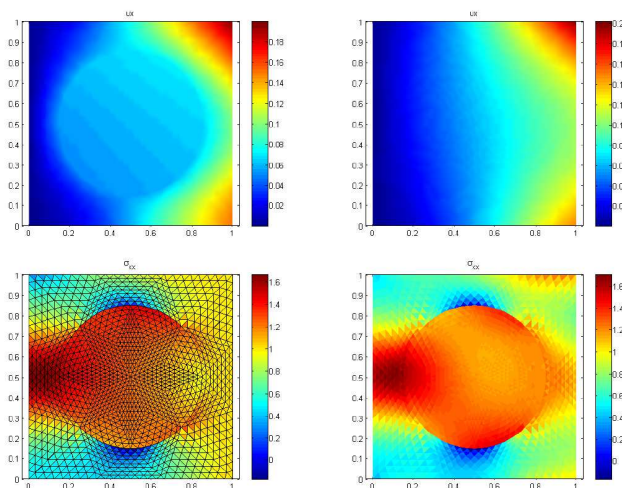


Figure 2.8: Test 2. Displacements (top row) and stresses (bottom row) obtained by fine mesh with 2900 (left column) and coarse mesh with 32 (right column) dof.

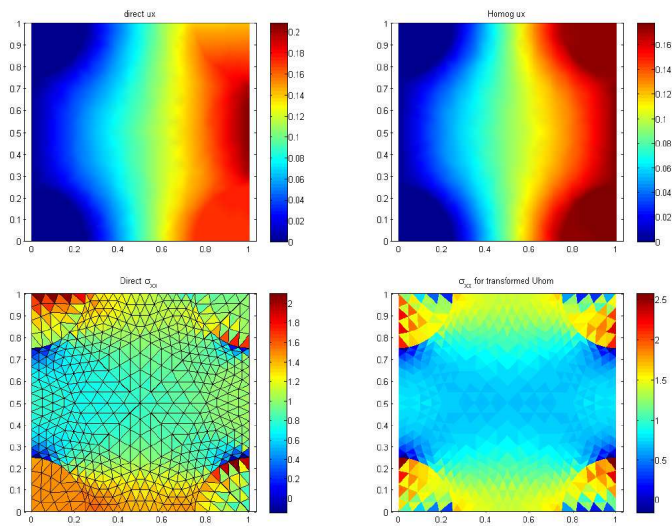


Figure 2.9: Test 3. Displacements (top row) and stresses (bottom row) obtained by fine (left column) and coarse (right column) meshes.

## 2.4 Coupled problems

The weakly coupled problem that models mechanical deformations resulting from both statical loading and steady state heat flow is considered in this section and is analyzed by the multigrid homogenization method since both mechanical and thermal material properties are rapidly varying in the considered domain. Thus, our problem reads: *find fields of displacements  $\mathbf{u}(\mathbf{x})$  and temperature  $\theta(\mathbf{x})$  such that:*

$$\begin{aligned} -\frac{\partial}{\partial x_j} \left[ C_{ijkl}^\varepsilon \left( \frac{\partial u_k}{\partial x_l} - \alpha \theta \delta_{kl} \right) \right] &= f_i \quad \forall \omega_s \subset \Omega \\ -\frac{\partial}{\partial x_i} \left( k_{ij}^\varepsilon \frac{\partial \theta}{\partial x_j} \right) &= Q \quad \forall \omega_s \subset \Omega \end{aligned} \quad (2.14)$$

with mechanical Dirichlet ( $\hat{\mathbf{u}}$ ) and Neumann ( $\hat{\mathbf{t}}$ ) boundary conditions on  $\partial\Omega_D$  and  $\partial\Omega_N$  respectively ( $\partial\Omega_D \cup \partial\Omega_N = \partial\Omega$ ,  $\partial\Omega_D \cap \partial\Omega_N = \emptyset$ ) and thermal Dirichlet ( $\hat{\theta}$ ) and Neumann ( $\hat{q}$ ) boundary conditions on  $\partial\Omega_D$  and  $\partial\Omega_N$  respectively ( $\partial\Omega_D^\theta \cup \partial\Omega_N^\theta = \partial\Omega$ ,  $\partial\Omega_D^\theta \cap \partial\Omega_N^\theta = \emptyset$ ) as well as continuity conditions for mechanical and thermal fields and their gradients at the possible material interfaces  $\Gamma$ . We shall also assume  $L^2$  regularity of  $\mathbf{f}$  and  $Q$ , strong ellipticity and boundedness of the material parameter tensors  $C^\varepsilon$ ,  $\mathbf{k}^\varepsilon$ , where superscript  $\varepsilon$  indicates that the ratio of the smallest and largest scales in the problem may be small  $\varepsilon \ll 1$  and  $\omega_s$  for  $s = 1, \dots, N$ ,  $\sum_s \omega_s = \Omega$ , denotes  $i$ -th subdomain in which material parameters are differentiable (typically constant).

The corresponding weak formulation of problem (2.14) is as follows: *find fields of displacements and temperature  $\mathbf{u}(\mathbf{x}) \in \mathbf{V}_0 + \hat{\mathbf{u}}$ ,  $\theta \in V_0 + \hat{\theta}$ , such that:*

$$\begin{aligned} \int_\Omega \boldsymbol{\varepsilon}(\mathbf{v}) : \boldsymbol{\sigma}(\mathbf{u}) \, d\Omega - \int_\Omega \boldsymbol{\varepsilon}(\mathbf{v}) : \boldsymbol{\varepsilon}^* \, d\Omega &= \int_\Omega \mathbf{f} \cdot \mathbf{v} \, d\Omega + \int_{\partial\Omega_N} \hat{\mathbf{t}} \cdot \mathbf{v} \, ds \quad \forall \mathbf{v} \in \mathbf{V}_0 \\ \int_\Omega \nabla \psi \mathbf{k} \nabla \theta \, d\Omega &= \int_\Omega Q \psi \, d\Omega + \int_{\partial\Omega_N} \hat{\theta} \cdot \psi \, ds \quad \forall \psi \in V_0 \end{aligned} \quad (2.15)$$

where  $\mathbf{V}_0 = \{\mathbf{v} \in [H^1(\Omega)]^n, \mathbf{v} = 0 \text{ on } \partial\Omega_D\}$ ,  
 $V_0 = \{v \in [H^1(\Omega)], v = 0 \text{ on } \partial\Omega_D^\theta\}$ ,  $\boldsymbol{\varepsilon}_{ij}^* = \alpha \theta \delta_{ij}$ .

Similarly as in the case of purely mechanical problem the interpolation operator is computed in two steps.

In the first step the edge values  $\hat{\varphi}$  are obtained for every nonzero trace of all coarse element scalar shape functions  $\psi$  as the solution to the following 1D

boundary value problem

$$\begin{aligned} \frac{d}{ds}(2\mu + \lambda) \frac{d\hat{\varphi}}{ds} - \frac{d}{ds}(2\mu + \lambda)\alpha\theta &= \text{Reg} \left[ \frac{d}{ds}(2\mu + \lambda) \frac{d\psi}{ds} - \frac{d}{ds}(2\mu + \lambda)\varphi ds \right] \text{ in } (0, l) \\ \frac{d}{ds}k \frac{\hat{\theta}}{ds} &= \text{Reg} \left( \frac{d}{ds}k \frac{\hat{\theta}}{ds} \right) \\ \hat{\varphi}(0) = \psi(0), \quad \varphi(l) = \psi(l) \end{aligned} \quad (2.16)$$

where  $\text{Reg}$  denotes regular part of the derivative, i.e. without distributional part and  $s \in [0, l]$  stands for the parameter that defines an edge. The coefficient  $2\mu + \lambda$  represents material properties along an edge.

In the second step for every vector valued shape function  $\Psi$  its vector valued interpolant  $\Phi$  is computed by solution of the Dirichlet boundary value problem analogical to (2.5).

## 2.5 Numerical examples

In this section we present results of experimentally studied accuracy and convergence for high order FEM in multigrid homogenization applied for thermo-mechanical problem. The test problem is defined in Fig. 2.10. The results are shown in Figs. 2.12-2.15 showing suitability of the multigrid homogenization for taking into account thermal effects in multiscale analysis.

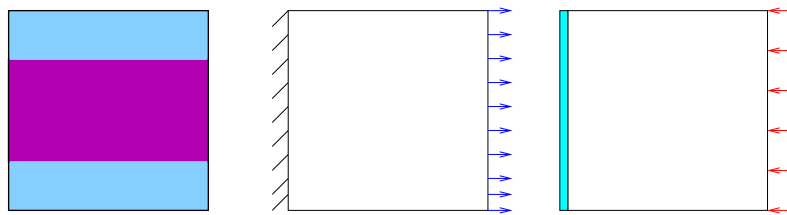


Figure 2.10: Thermomechanical test problem. Heterogeneous domain, mechanical boundary conditions (zero Dirichlet along the left edge and Neumann along the other edges) and thermal conditions (also zero Dirichlet along the left edge and Neumann along the other edges).

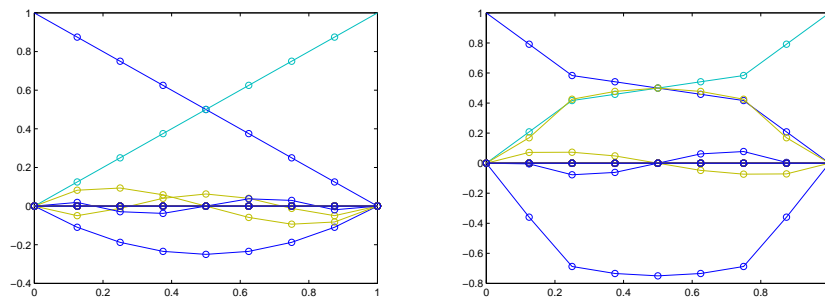


Figure 2.11: Coupled thermomechanical test problem. Interpolants of the coarse shape functions along the vertical, right-hand side edge for homogeneous and heterogeneous materials.

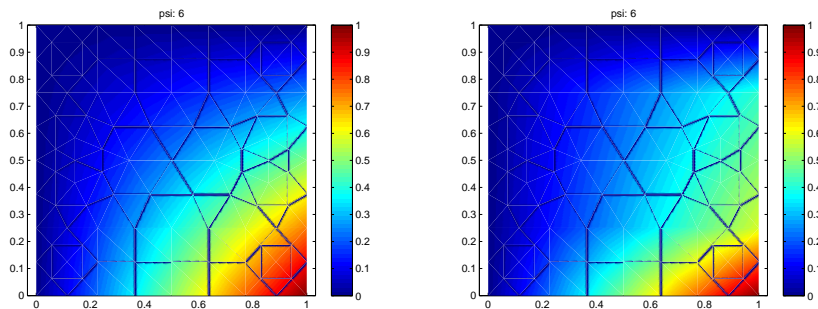


Figure 2.12: Coupled thermomechanical test problem. Countour plots of a selected coarse shape function for homogeneous and heterogeneous materials.

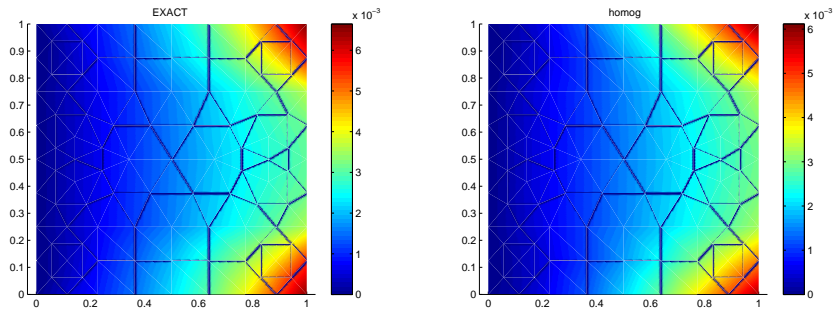


Figure 2.13: Coupled thermomechanical test problem. Countour plots of directly computed horizontal displacement ("exact") and its multigrid homogenization based approximation.

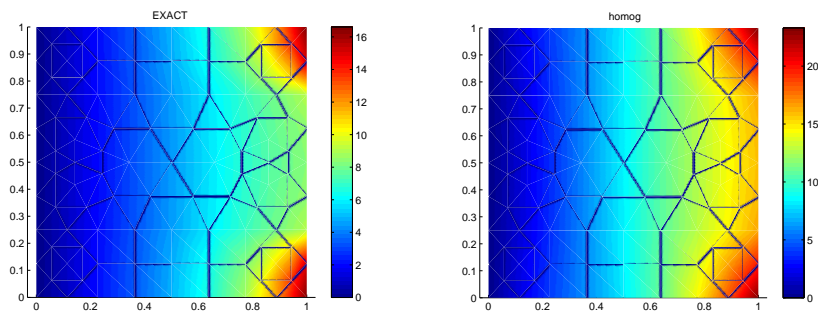


Figure 2.14: Coupled thermomechanical test problem. Countour plots of directly computed temperature ("exact") and its multigrid homogenization based approximation.

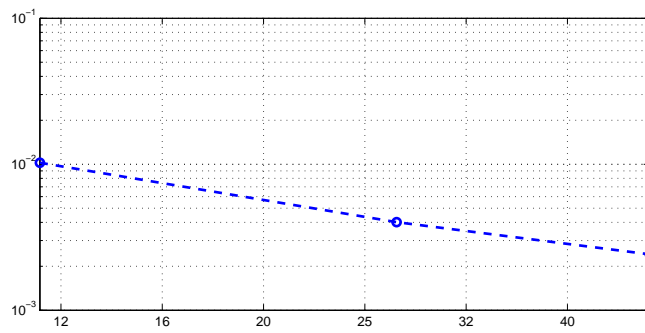


Figure 2.15: Coupled thermomechanical test problem. Convergence of the modeling error of the multigrid homogenization.

## Chapter 3

# Mixed finite elements

The finite elements in which the displacements and stress fields are approximated independently are called mixed ones. Since, contrary to the displacement version, the stresses are not computed by differentiation of the primary variable their accuracy and convergence are better. Moreover, mixed elements can easily handle problems with an incompressible material.

Applications of mixed finite elements have been developed since the seventies. Let us only mention works done by Brezzi [9], Babuska [5], Crouzeix and Raviart [13], Raviart and Thomas [23] or Arnold [3, 2, 4].

In the multiscale analysis the stresses are of particular interest, thus we studied efficiency of mixed finite elements for both elastic and elastic-plastic problems.

### 3.1 Two-dimensional mixed hp-finite elements

A brief recapitulation of mixed finite element method after [12] is presented in this section.

Stable mixed finite elements for solid mechanics are very difficult to construct since they have to provide symmetry and continuity of tractions only. We have applied the approximation with weakly imposed symmetry [22] expecting the following advantages

- good coarse mesh accuracy for stresses
- no problems with incompressible material ( $\nu = 0.5$ )
- no sensitivity against mesh distortions
- no sensitivity against heterogeneous materials with significantly different material properties

The equations of linear elasticity may be written in the following form

$$\begin{cases} \boldsymbol{\varepsilon}(\mathbf{u}) = \mathbf{C}^{-1}\boldsymbol{\sigma} & \text{w } \Omega \\ \mathbf{div } \boldsymbol{\sigma} = -\mathbf{b} & \text{w } \Omega \\ \mathbf{u} = 0 & \text{na } \partial\Omega_D \\ \boldsymbol{\sigma}\mathbf{n} = \hat{\mathbf{t}} & \text{na } \partial\Omega_N \end{cases} \quad (3.1)$$

where:

$\mathbf{u}$  – displacement field

$\boldsymbol{\sigma}$  – stress field

$\boldsymbol{\varepsilon}$  – strain field

$\mathbf{C}$  – material parameter tensor

$\mathbf{b}$  – body forces

$\mathbf{n}$  – unit outward normal vector

$\hat{\mathbf{t}}$  – boundary loading

The corresponding weak formulation is the Hellinger–Reissner principle  
Find  $\boldsymbol{\sigma} \in \mathbf{H}_q(\text{div}, \Omega, \mathbf{S})$  i  $\mathbf{u} \in L^2(\Omega, \mathbf{V})$ , such that:

$$\begin{cases} \int_{\Omega} \boldsymbol{\tau} : \mathbf{C}^{-1}\boldsymbol{\sigma} \, d\Omega + \int_{\Omega} \mathbf{div } \boldsymbol{\tau} \cdot \mathbf{u} \, d\Omega & = \int_{\partial\Omega} \boldsymbol{\tau} \mathbf{n} \cdot \hat{\mathbf{u}} \, ds \\ \int_{\Omega} \mathbf{v} \cdot \mathbf{div } \boldsymbol{\sigma} \, d\Omega & = - \int_{\Omega} \mathbf{v} \cdot \mathbf{b} \, d\Omega \end{cases} \quad (3.2)$$

$$\forall \boldsymbol{\tau} \in \mathbf{H}_0(\text{div}, \Omega, \mathbf{S}), \quad \forall \mathbf{v} \in L^2(\Omega)$$

where  $\boldsymbol{\tau} \in L^2(\Omega, \mathbf{S})$  i  $\mathbf{v} \in L^2(\Omega, \mathbf{V})$ ,  $\mathbf{S}$  is a space of symmetric tensors  $\mathbf{R}_{sym}^{n \times n}$  and  $\mathbf{V}$  is vector space  $\mathbb{R}^n$ .  $\mathbf{H}_q(\text{div}, \Omega, \mathbf{S})$  are stresses with divergence square integrable and tractions equal to  $\mathbf{q}$  to  $\partial\Omega_N$ ,  $\hat{\mathbf{u}}$  is trace of displacements along  $\partial\Omega_D$ ,  $\partial\Omega_D \cup \partial\Omega_N = \partial\Omega$ .

In the case of elastic-plastic deformations at every semi-time step the following problem is solved with known plastic strains  $\boldsymbol{\varepsilon}^p$

$$\begin{cases} \int_{\Omega} \boldsymbol{\tau} : \mathbf{C}^{-1}\boldsymbol{\sigma} \, d\Omega + \int_{\Omega} \mathbf{div } \boldsymbol{\tau} \cdot \mathbf{u} \, d\Omega & = \int_{\partial\Omega} \boldsymbol{\tau} \mathbf{n} \cdot \hat{\mathbf{u}} \, ds + \int_{\Omega} \boldsymbol{\tau} : \boldsymbol{\varepsilon}^p \, d\Omega \\ \int_{\Omega} \mathbf{v} \cdot \mathbf{div } \boldsymbol{\sigma} \, d\Omega & = - \int_{\Omega} \mathbf{v} \cdot \mathbf{b} \, d\Omega \end{cases} \quad (3.3)$$

For such a problem with additional plastic term we observed the same convergence rate for both displacements as well as stresses and the same as for the simpler problem (3.2) without the plastic strains.

The test functions may be selected by considering the following system of algebraic equations

$$\begin{bmatrix} \mathbf{A}_{m \times m} & \mathbf{B}_{m \times n} \\ (\mathbf{B}^T)_{n \times m} & \mathbf{0} \end{bmatrix} = \begin{bmatrix} \mathbf{c} \\ \mathbf{0} \end{bmatrix} \quad (3.4)$$

where  $m \geq n$ .

Stable approximation must satisfy the *inf-sup* condition [5] or commutativity of the de Rham diagram [10], i.e.

$$\begin{array}{ccc} C^\infty(\Omega, \mathbf{S}) & \xrightarrow{\text{div}} & C^\infty(\Omega, \mathbb{R}^2) \\ \downarrow \Pi_h & & \downarrow P_h \\ \Sigma_h & \xrightarrow{\text{div}} & V_h \end{array}$$

where  $\Pi_h, P_h$  are projection based interpolation operators.

Summing up the requirements for a stable mixed approximation are the following:

- stress tensor symmetry
- traction continuity
- piecewise continuity of displacements
- commutativity of the de Rham diagram
- local variation of approximation order
- possible adaptive mesh refinement

We have constructed the appropriate shape functions in two ways either by explicitly enforcing the continuity of tractions [12] or by using the exact sequence methodology. The later method is briefly described below and is a part of the research that is currently conducted on development of the new HP3D code.

## 3.2 Edge functions

The edge shape functions are defined by extending the 1D bubble shape functions defined on the edge to the element. For tensor product elements,

the extension involves use of a projection and the edge blending function, thus the functions are evaluated as the following product

$$\varphi = \psi(\xi_1, \xi_2) \hat{\chi}\{\xi^e[t^e(\xi_1, \xi_2)]\} \quad (3.5)$$

where:  $\psi$  is a blending function for the edge,  $\chi$  denote 1D shape functions defined along the edge,  $t^e$  is the local coordinate defining projection of point  $(\xi_1, \xi_2)$  onto the edge,  $\xi^e$  stands for the corresponding global edge coordinate.

Thus projection and accounting for orientation are the two important steps here. They are illustrated in Fig. 3.1.

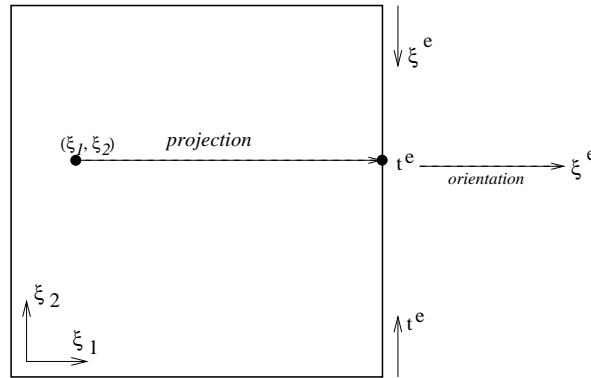


Figure 3.1: Illustration of projection and edge orientation in a quad.

Eq. (3.5) implies that

$$\frac{\partial \varphi}{\partial \xi_i} = \frac{\partial \psi}{\partial \xi_i} \chi + \psi \frac{d\hat{\chi}}{d\xi^e} \frac{d\xi^e}{dt^e} \frac{\partial t^e}{\partial \xi_i} \quad (3.6)$$

The following routines are used to compute both  $\varphi$  and  $\frac{\partial \varphi}{\partial \xi_i}$

- *blend\_quad* - for  $\psi, \frac{\partial \psi}{\partial \xi_i}$
- *project\_quad2e* - for  $t^e, \frac{\partial t^e}{\partial \xi_i}$

### 3.3 Bubble functions

These functions are evaluated as the following (tensor) products

$$\varphi = \chi_1(\xi_1^f) \chi_2(\xi_2^f) \quad (3.7)$$

where:  $\chi_k$  denote 1D bubble shape function (in  $k - th$  direction).

There are 8 possible orientations of a quad. They may written in the following general form

$$\xi^f = \xi^f(\mathbf{t}^f) \quad (3.8)$$

Whenever the orientation should be accounted for, then the following chain rule must be used to compute derivatives

$$\frac{\partial \varphi}{\partial t_i^f} = \frac{\partial \hat{\varphi}}{\partial \xi_k^f} \frac{\partial \xi_k^f}{\partial t_i^f} \quad (3.9)$$

where:  $\hat{\varphi}$  denotes a bubble function in domain  $[0, 1] \times [0, 1]$

### 3.4 Numerical tests

A square  $2mm \times 2mm$  domain with square like  $1mm \times 1mm$  inclusion located in the center was analyzed constant distributed loading  $q = 100 kN/m$ . Due to the symmetry only a quarter of that domain wa considered as shown in Fig. 3.2. The matrix Young modulus was  $E = 200 GPa$  and its Poisson ratio  $\nu = 0.3$ . Inclusion parameters were  $E = 200 MPa$  and  $\nu = 0.3$ .

The results obtained for both ways of deriving the shape functions were teh same and are shown in Figs. 3.3, 3.4. All these results confirm efficiency of the proposed version of the mixed hp-FEM.

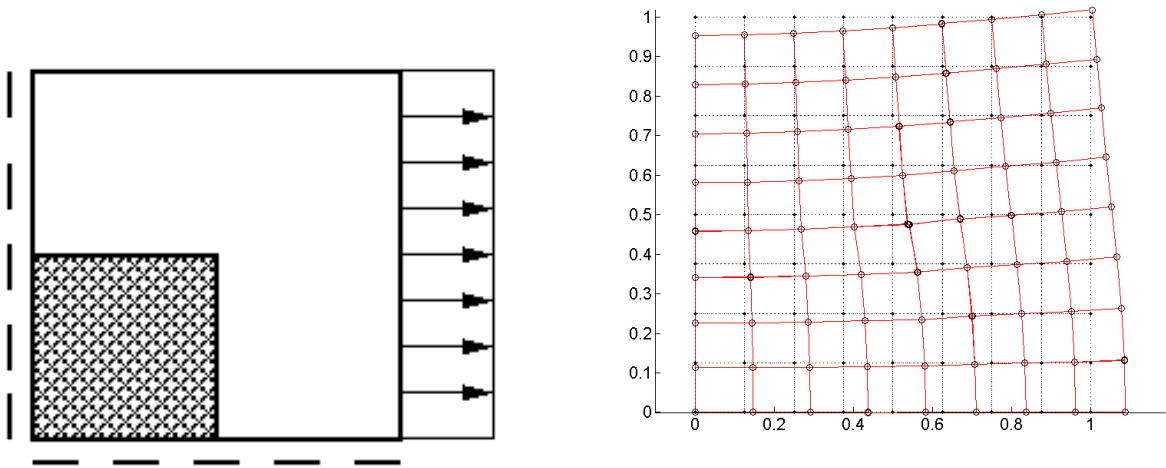


Figure 3.2: RVE with square like inclusion. Problem set up and deformations.

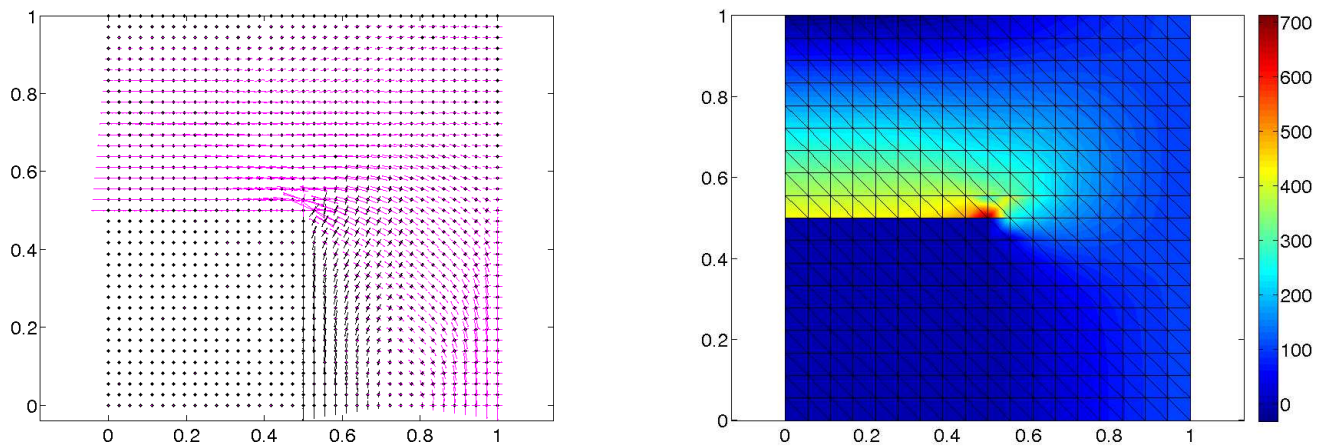


Figure 3.3: RVE with square like inclusion. Principal stresses and contour lines of  $\sigma_{xx}$ .

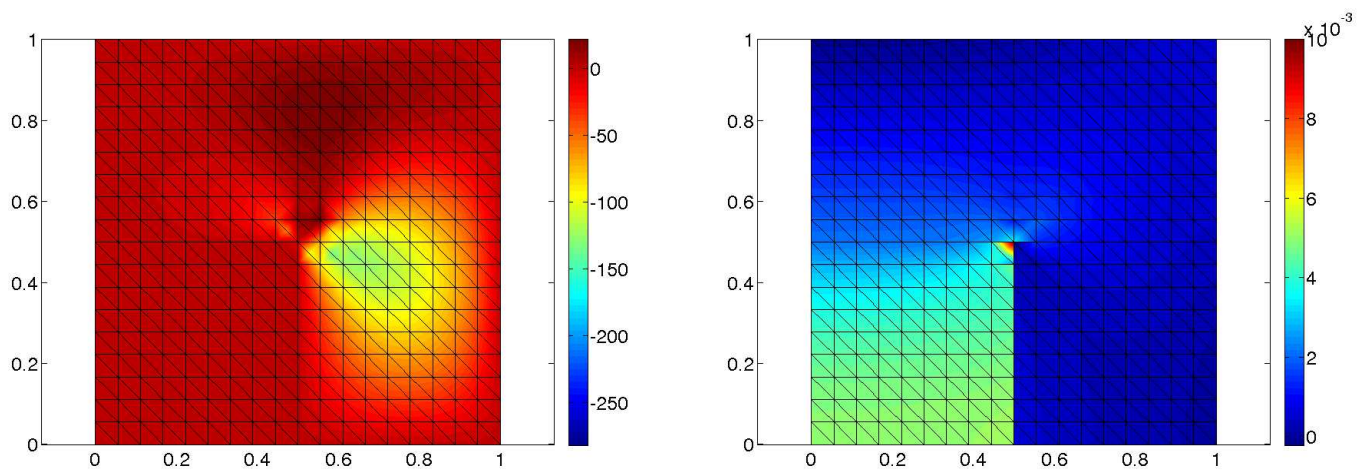


Figure 3.4: RVE with square like inclusion.  $\sigma_{yx}$  and  $\epsilon_{xx}$ .

## Chapter 4

# Concluding remarks

We have applied the hierarchical approximation of order up to 5 for multigrid homogenization using a new method of the intergrid mapping construction. Whenever these mappings are well defined the coarse element stiffness matrices and load vectors are computed by multiplication of previously evaluated matrices and vectors without necessity for additional integration. The numerical experiments show a fast reduction of modeling error that is inevitably introduced by the homogenization. The fast convergence is observed for both displacements and stresses while higher order of coarse scale bases are used. We also pointed out that the multigrid homogenization is equivalent to the MsFEM. Further development of this type of homogenization will include application to physically and geometrically nonlinear problems as well as more than two grid coarsening.

Also possibilities and advantages of the mixed FEM for elastic-plastic analysis with heterogeneous material were presented in this report. Two methods of construction of appropriate  $H(div)$  shape functions were used and gave the same convergence rates for displacements and stresses with or without plastic strains for a selected numerical example.

# Bibliography

- [1] R. Alcouffe, A. Brandt, J. Dendy Jr., and J. Painter. The multi-grid method for the diffusion equation with strongly discontinuous coefficients. *SIAM J. Sci. Statist. Comput.*, 4:430–454, 1981.
- [2] D. N. Arnold, G. Awanou, and R. Winther. Finite elements for symmetric tensors in three dimensions. *Mathematics of Computations*, 77(263):1229–1251, 2008.
- [3] D. N. Arnold, D. Boffi, and R. Falk. Quadrilateral  $H(\text{div})$  finite elements. *SIAM J. Numer. Anal.*, 42(6):2429–2451, 2005.
- [4] D. N. Arnold, R. Falk, and R. Winther. Mixed finite element methods for linear elasticity with weakly imposed symmetry. *Mathematics of Computations*, 76(260):1699–1723, 2007.
- [5] I. Babuška. The finite element method with Lagrangian multipliers. *Numer. Math.*, 20:179–192, 1973.
- [6] I. Babuška, G. Caloz, and J. Osborn. Special finite element method for a class of second order elliptic problems with rough coefficients. *SIAM J. Num. Anal.*, 31:945–981, 1994.
- [7] H. Boffy and C Venner. Multigrid solution of the 3D stress field in strongly heterogeneous materials. *Tribology International*, 74:121–129, 2014.
- [8] A. Brandt. A multi-level adaptive technique (MLAT) for partial differential equations: ideas and software. *Math. Softw.*, 3:273–314, 1977.
- [9] F. Brezzi. On the existence, uniqueness and approximation of saddle-point problems arising from lagrangian multipliers. *Rev. Francaise Automat. Informat. Recherche Operationnelle Ser. Rouge*, 8(151):129–211, 1974.

- 
- [10] F. Brezzi and L.D. Marini. A survey on mixed finite element methods. *IEEE Transactions on Magnetics*, 30(5):3547–3551, 1994.
- [11] W. Cecot and M. Oleksy. High order FEM in multigrid homogenization. *Computers and Mathematics with Applications*, submitted.
- [12] W. Cecot, M. Serafin, I. Jaworska, M. Klimczak, S. Milewski, and W. Rachowicz. Wieloskalowe modelowanie niesprezystych materialow heterogenicznych za pomoca; hp-adaptacyjnej metody elementow skonczonych. Technical Report B/163/2010, Institute for Computational Civil Engineering, Cracow University of Technology, 2010.
- [13] M. Crouzeix and P. A. Raviart. Conforming and nonconforming finite element methods for solving the stationary Stokes equations. *R.A.I.R.O. R3*, 7:33–76, 1973.
- [14] Y. Efendiev and T. Hou. Multiscale finite element methods for porous media flows and their applications. *Appl. Num. Math.*, 57:577–596, 2007.
- [15] Y. Efendiev and T. Hou. *Multiscale Finite Element Methods. Theory and Applications*. Springer, 2009.
- [16] R. Hoekema, K. Venner, J. Struijk, and J. Holsheimer. Multigrid solution of the potential field in modeling electrical nerve stimulation. *Computers and Biomedical Research*, 31:348–362, 1998.
- [17] T. Hou and X. Wu. A multiscale finite element method for elliptic problems in composite materials and porous media. *J. Comp. Phys.*, 134:169–189, 1997.
- [18] V. Kouznetsova. *Computational homogenization for the multi-scale analysis of multi-phase materials*. PhD thesis, Technische Universiteit, Eindhoven, 2002.
- [19] J. Moulton, J. Dendy, and J. Hyman. The black box multigrid numerical homogenization algorithm. *J. Comp. Phys.*, 141:1–29, 1998.
- [20] J. Moulton, S. Knapek, and J. Dendy. Multilevel upscaling in heterogeneous porous media. <http://math.lanl.gov/moulton/papers/homogenization/cnls-1999-01.pdf>, 1999.
- [21] N. Neuss, W. Jager, and G. Wittum. Homogenization and multigrid. *Computing*, 66:1–26, 2001.

- 
- [22] W. Qiu and L. Demkowicz. Mixed hp-finite element method for linear elasticity with weakly imposed symmetry. *Comp. Meth. Appl. Mech. Engng*, 198:3682–3701, 2009.
- [23] P. A. Raviart and J. M. Thomas. A mixed finite element method for 2-nd order elliptic problems. In A. Dold and B. Eckmann, editors, *Mathematical Aspects of Finite Element Methods*, pages 292–315. Springer:Berlin, 1977.
- [24] S. Soghrati and I. Staniulescu. Systematic construction of higher order bases for the finite element analysis of multiscale elliptic problems. *Mechanics Research Communications*, 52:11–18, 2013.